arXiv:2404.04655v1 [cond-mat.mtrl-sci] 6 Apr 2024

Insights on induced magnetic moments and spin textures in synthetic ferrimagnetic Pt/Co/Gd heterolayers

J. Brandão,[*,†] P. C. Carvalho,[‡] I. P. Miranda,[*,¶] T. J. A. Mori,[†] F. Béron,[§] A. Bergman,[¶] H. M. Petrilli,[‡] A. B. Klautau,[‖] and J. C. Cezar[†]

†*Laboratório Nacional de Luz Síncrotron, Centro Nacional de Pesquisa em Energia e Materiais, 13083-970 Campinas SP, Brazil*

‡*Universidade de São Paulo, Instituto de Física, Rua do Matão, 1371, 05508-090 São Paulo, São Paulo, Brazil*

¶*Department of Physics and Astronomy, Uppsala University, 75120 Box 516 Sweden*

§*Instituto de Física Gleb Wataghin, Universidade Estadual de Campinas,13083-859 Campinas SP, Brazil*

‖*Faculdade de Física, Universidade Federal do Pará, CEP 66075-110, Belém, PA, Brazil*

E-mail: jeovani.brandao@lnls.br; ivan.miranda@alumni.usp.br

Abstract

To develop new devices based on synthetic ferrimagnetic (S-FiM) heterostructures, understanding the material's physical properties is pivotal. Here, the induced magnetic moment (IMM), magnetic exchange-coupling, and spin textures were investigated at room-temperature in Pt/Co/Gd multilayers using a multiscale approach. The magnitude and direction of the IMM were interpreted experimentally and theoretically in the framework of both X-ray magnetic circular dichroism (XMCD) and density functional theory (DFT). The results demonstrate that the IMM transferred by Co across the Gd paramagnetic (PM) thickness leads to a flipped spin state (FSS) within the Gd layers, in which their magnetic moments couple antiparallel/parallel with the ferromagnetic (FM) Co near/far from the Co/Gd interface, respectively. For the Pt, in both Pt/Co and Gd/Pt interfaces the IMM follows the same direction as the Co magnetic moment, with negligible IMM in the Gd/Pt interface. Additionally, zero-field spin spirals were imaged using scanning transmission X-ray microscopy (STXM), while micromagnetic simulations employed to unfold the interactions stabilizing the FiM configurations, where the existence of a sizable Dzyaloshinskii-Moriya interaction is demonstrated to be crucial for the formation of those spin textures. Our outcomes may add fundamental physical and technological aspects for using FiM films in antiferromagnetic spintronic devices.

Introduction

Interface-induced properties in thin films and multilayers have been considered to play an important role in different processes, including spin transport, interfacial anisotropy, topological superconductivity, and proximity effect.[1–4] The latter is known for transferring electronic properties to other materials where it is not present themselves. For instance, the surface/interface of a certain material without electronic order may acquire superconductivity and ferromagnetism in contact with superconductors or ferromagnets, respectively.[5–9] So far, particularly, induced magnetic mo-

ment (IMM) has been investigated mostly in ferromagnetic/non-magnetic interfaces, where the magnetization of $3d$ transition metals (Co, Fe, Ni) induces a magnetic polarization in $4d$ (Pd), $5d$ heavy metals (W, Ir, Pt) when they are thin and in proximity.[10,11]

Only in the last few years, IMM has gathered more attention in ferrimagnetic systems[12–14] due to the advantages of several magnetic processes compared to the correlative ferromagnetic, as exemplified by all-optical switching (AOS),[15,16] suppression of skyrmion Hall effect,[17,18] faster domain wall motion[19] and THz dynamics.[20,21] Single shot pulsed laser with a few picosecond time scale driving magnetization reversal and topological spin textures nucleation such as skyrmions has been observed in ferrimagnetic films even without the assistance of magnetic fields.[22–26] These mechanisms place ferrimagnets as an energy-efficient material for nonvolatile ultrafast toggle switching to develop antiferromagnetic spintronics devices.[27–29]

Thin films and multilayers composed of Co and Gd alloy or bi-layers made of Co/Gd are examples of ferrimagnetic coupling where the Co $3d$ transition metal and Gd $4f$ rare-earth magnetic moments may align antiferromagnetically concerning each other depending on the composition and temperature.[30] This antiparallel alignment emerges due to an *indirect* negative exchange played by the bridge role, which essentially means that the Gd $5d$ and $4f$ magnetic moments are parallel via direct exchange (or via a polarizing field generated by the localized f-states, when they are theoretically treated as part of the core), however, are antiparallel to the Co $3d$ magnetic moments through the hybridization of the itinerant $5d-3d$ states.[31]

When Pt is added as an under/over layer in CoGd alloys or Co/Gd bi-layer, its IMM physical understanding remains under debate. Pt is a heavy paramagnetic material with an electronic band structure that may satisfy the Stoner criterion to acquire ferromagnetic order. Therefore, Pt does not exhibit spontaneous magnetic polarization, except when occurs size reduction or proximity with a ferromagnetic material.[32,33] Besides, an important question arises about the magnetic polarization for Pt in contact with rare-earth elements such as Gd, which calls attention to the role played by Gd-Pt ($5d-5d$ and $4f-5d$) interaction in transferring IMM. To quantify the IMM and its implication on the interfacial magnetic properties of various phenomena occurring in multilayered materials, advanced experimental techniques with chemical selectivity in combination with theoretical models are key tools to identify the direction, magnitude, and effects of the IMM.

In this work, element-resolved magnetic moment was probed in Pt/Co/Gd heterolayers. By means of XMCD, magnetic moments were detected individually for each element. IMM transferred from Co to Pt and Gd was measured at room-temperature. From the average XMCD signal, experimentally, both magnetic moments in the Co and Pt are aligned parallel with the external magnetic field direction. On the other hand, the magnetic polarization in the Gd is anti-parallel with respect to the magnetic field. Using well-known sum rules the magnitude of the orbital and spin magnetic moments were experimentally determined, and to compare with theoretical values, density functional theory was employed. The theoretical results resolved layer-by-layer for each element show that the IMM in the Gd layer near the Co/Gd interface is coupled antiferromagnetically with the Co, whereas the Gd layers far from the Co/Gd interface are coupled ferromagnetically. Thus, herein this behavior designated as a flipped spin state (FSS) stands as an interface effect where an antiferromagnetic coupling occurs between interfacial Co and Gd atoms. This contrasts with the ferromagnetic configuration observed within the Gd below the Curie temperature in the absence of Co, in which FSS does not appear. This theoretical achievement of FSS within the Gd layer is further reinforced by comparing the average experimental and theoretical magnetic moments. In addition, scanning transmission X-ray microscopy reveals the formation of antiferromagnetic coupled spin spirals as the magnetic configurations at the nanoscale in the multilayer. Micromagnetic simulations were performed to reproduce the experimental images and understand the

energy landscape leading to such spin textures.

Results and Discussions

Room-temperature magnetism in Pt/Gd and Pt/Co multilayers. Hysteresis loops were measured for the two reference multilayers Pt(1nm)/Gd(1nm) and Pt(1nm)/Co(1nm), see Figure 1(a) and (e) using a vibrating magnetometer sample (VSM) with an applied magnetic field along the out-of-plane direction. In Figure 1(b), magnetization reversal acquired for the Pt(1nm)/Gd(1nm) multilayer shows a typical behavior of a paramagnetic material, where the magnetization slowly increases for higher magnetic fields, but does not reach saturation. This is expected for the Pt/Gd multilayer, since Gd bulk is paramagnetic above 292 K, whereas the Curie temperature might be even lower for thin Gd films. To confirm the paramagnetic nature of the Gd film, element-specific X-ray absorption spectroscopy (XAS) and X-ray magnetic circular dichroism (XMCD) were performed at room-temperature using a superconducting magnet installed at the Planar Grating Monochromator (PGM) beamline of the UVX Brazilian Synchrotron Light Laboratory (LNLS) of the Brazilian Center for Research in Energy and Materials (CNPEM).

XAS was acquired with the incoming X-ray and magnetic field of 1 T normal to the sample surface. The signal was detected in the total electron yield (TEY) mode. Figure 1(c) shows two X-ray spectra acquired with right (μ^+) and left (μ^-) circularly polarized X-ray. It shows no dependence of the XAS intensity to the X-ray polarization (μ^+, μ^-). In Figure 1(d), the resultant XMCD ((μ^+) - (μ^-)) shows a typical derivative signal (asymmetric line shape) confirming that the Gd present in the Pt/Gd multilayer is not ferromagnetic at ambient conditions.

Hysteresis loops were then acquired for the Pt(1nm)/Co(1.5nm), as shown in Figure 1(f). As expected, it shows a magnetization reversal characteristic of Pt/Co perpendicular multilayers. Even so, XAS and XMCD were also acquired at room temperature to obtain the individual magnetism of the Co, where can be seen the dependent X-ray absorption for the X-ray polarization in Figure 1(g). In Figure 1(h), the resultant XMCD points downwards/upwards around the L_3 and L_2 absorption edges, correspondingly. Therefore, at room-temperature, the Pt/Gd multilayer is paramagnetic while the Pt/Co is ferromagnetic. It is worth anticipating that simulations for the Pt/Co/Pt multilayers were performed to establish the methodology used for comparing theoretical and experimental results since this system is well-known in the literature.[34,35] Through first-principles calculations and atomistic spin dynamics (ASD), a good agreement for the atomic Co magnetic moment was obtained (for more details, see SI).

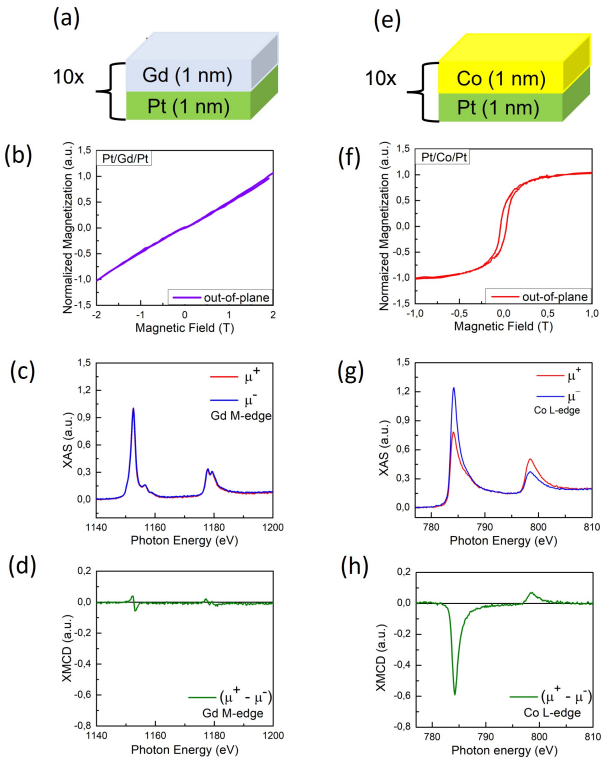

Figure 1: Reference multilayers Pt/Gd (a) and Pt/Co (e). In (b) for Pt/Gd the hysteresis loops show a paramagnetic behavior at room-temperature confirmed by the XAS (c) and XMCD (d). In (f), hysteresis loops performed for Pt/Co show magnetization reversal typical of a perpendicularly magnetized multilayer, which is confirmed by the XAS (g) and XMCD (h).

Induced magnetic moment in rare-earth

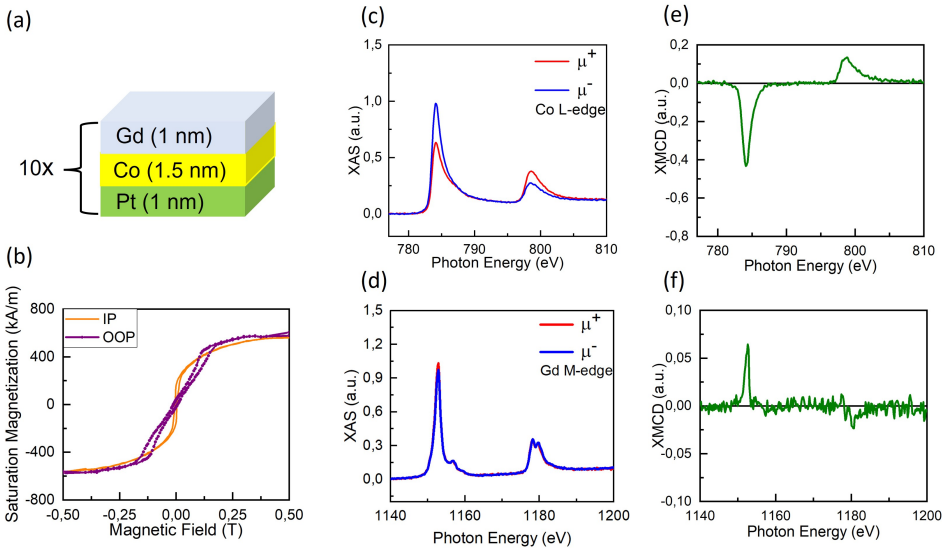

Figure 2: Sample stack, hysteresis loops, and XAS/XMCD measurements. In (a), a schematic representation of the Pt/Co/Gd heterolayer, corresponding to one stacking unit (to be repeated 10×). In (b) the hysteresis loops are acquired for both in-plane (IP) and out-of-plane (OOP) magnetic fields. In (c) and (d) the XAS acquired for right and left circularly polarized X-rays around the Co and Gd absorption edges, respectively. In (e) and (f) the resultant XMCD for Co and Gd.

Gd layers. The IMM was investigated in rare-earth Gd by introducing a thin Co (1.5 nm) thickness, thus forming a Pt/Co/Gd multilayer. X-ray diffraction was measured to investigate the structural growth of the sample. The films were grown in the textured [1 1 1] direction, as shown in Figure S1 in the Supporting Information (SI). Figure 2(a) shows a schematic representation of the Pt(1nm)/Co(1.5nm)/Gd(1nm) stack. The three-layers were repeated 10 times, thus above Gd there is Pt forming Pt/Co and Gd/Pt interfaces in the heterostructure. XAS and XMCD were performed for the Co, Gd, and Pt layers. Figure 2(b) shows the hysteresis loops acquired with in-plane and out-of-plane magnetic fields. From the reversal magnetization driven by the magnetic field is possible to infer that the heterostructure exhibits perpendicular magnetic anisotropy (PMA). Figure 2(c) depicts clearly the dependent XAS concerning the X-ray polarization acquired around the $L_{2,3}$ Co absorption edges and, in Figure 2(e), its respective XMCD. As it was observed for the reference Pt/Co multilayer the XMCD also points down/up around the L_3 and L_2 edges.

The same measurement was carried out for the Gd to investigate if the IMM is coming from the proximity with the Co layer. Figure 2(d) shows the spectra acquired around the $M_{5,4}$ Gd edges when the Gd is in contact with the 1.5 nm Co layer. Contrary to the observed in the Pt/Gd multilayer, the spectra show dependent absorption of opposite X-ray polarization, which is confirmed by the XMCD shown in Figure 2(f). Moreover, opposite to the observed in the Co layer, the average XMCD points downwards/upwards around the $M_{5,4}$ Gd edges. This means that the average Co and Gd magnetic moments are parallel/antiparallel to the magnetic field. Therefore, the Gd acquires an average IMM at room-temperature, with opposite direction compared to the Co.

Co and Gd atomic magnetic moments evaluated by sum rules. To assess and separate the orbital and spin magnetic moments for both Co and Gd layers, the well-known sum rules were employed by integrating the XAS and XMCD spectra for each element – see details in Figure S2 (SI). In Figure 3(a,c) and Figure 3(b,d) are presented the integrated XMCD and XAS for both Co and Gd spectra. Specif-

ically, for the integral performed over the Gd XMCD spectra, the parameter q could not be represented since the integral goes almost to zero (Figure 3(c)), which may be due to the half full Gd $4f$ shell.[36] For the Co, the average orbital and spin magnetic moments were quantified as 0.12 ± 0.02 and 1.45 ± 0.02 μ_B/atom, while for Gd -0.03 ± 0.01 and -0.54 ± 0.03 μ_B/atom.

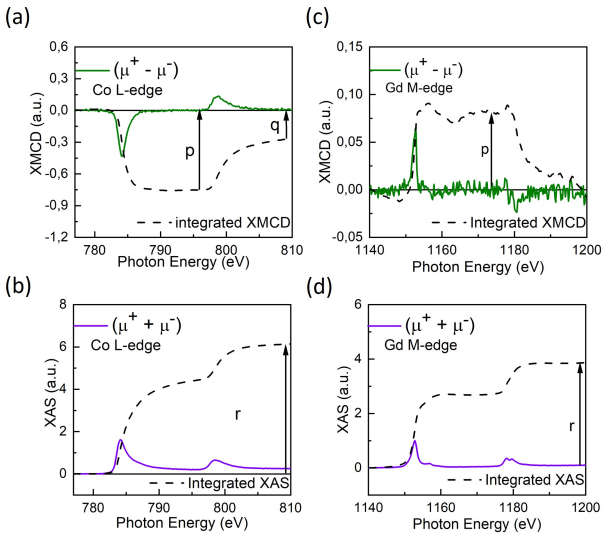

Figure 3: Integrated XAS and XMCD for both Co and Gd elements. Quantities p, q, and r are used to extract orbital and spin magnetic moments. Figure S2 in SI shows the extracted parameters in more detail.

This implies that the IMM within the Gd layers is about one-third of the Co magnitude. The observation calls attention to the range in which the magnetic moments of Co can induce polarization across the Gd thickness. This aspect will be later inspected via *ab-initio* calculations. In addition, the vanishing Gd orbital magnetic moment indicates that the perpendicular magnetization in the multilayer is dominated mostly by Co.

Induced magnetic moment at the Pt/Co and Gd/Pt interfaces. To fully understand the IMM in the multilayer, XAS and XMCD were also performed around the Pt $L_{2,3}$ absorption edges. XAS was measured in the hard X-ray energy range at the Extreme condition Methods of Analysis (EMA) beamline of the new 4th synchrotron generation Sirius. Right and Left circularly polarized X-rays were generated by 1/4 wave plate, and a magnetic field of 1 T perpendicular to the sample was applied during the XAS measurements. The signal was recorded in the fluorescence mode.

Figure 4(a) shows the XAS acquired for both incoming right and left circular polarization. It shows a difference in absorption around both L_2 and L_3 edges, which is observed in the XMCD signal in Figure 4(b). The XMCD points downwards/upwards around the L_3 and L_2 absorption edges, respectively. Figure 4(c) exhibits the sum of the XAS for right and left circularly polarized X-rays. Sum rules were also used to quantify the magnetic moment in the Pt layer. The average orbital and spin magnetic moments were obtained as 0.026 ± 0.01 μ_B/atom and 0.09 ± 0.04 μ_B/atom, respectively.

Theoretical analysis: Atomistic modelling. To uncover the physical aspects driving the IMM into the Gd and Pt layers at the interface, the Pt/Co/Gd system was investigated via a combination of first-principles calculations based on density functional theory (DFT) and ASD simulations for different temperatures (see Methods section).

The layer-resolved atomic spin magnetic moments (μ_s) are displayed in Figure 5(a), and the corresponding static average spin ($\bar{\mu}_s^z$) magnetic moments for the Pt, Co, and Gd atoms for $T = 0$ K are presented in Table 1. At the ground-state, our results show that the Gd dominates the magnetism in absolute values, presenting a spin magnetic moment very close to its measured bulk value (7.63 μ_B/atom[37]). As can be seen in Figure 5(a), within the Gd thickness, the two layers closest to the Co/Gd interface align antiferromagnetically to the Co spin state, while the two layers farthest to that interface present a ferromagnetic alignment with Co, characterizing the FSS state. This reduces the overall ground-state average magnetic moment of Gd to almost zero (see Table 1). Indeed, the temperature-dependent magnetic moment extracted for Co and Gd summarizes this behavior in which the resultant magnetic moment for the Gd at $T \to 0$ tends to vanish (data

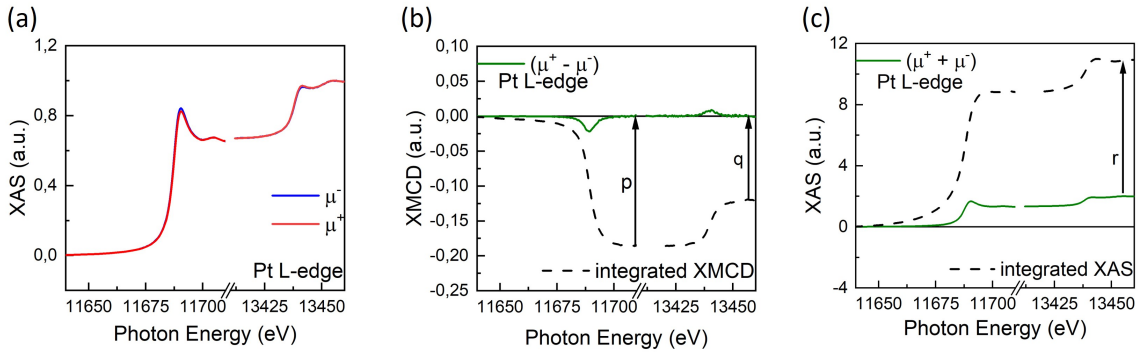

Figure 4: XAS and XMCD performed around the Pt $L_{2,3}$ edges. In (a), the XAS acquired for right and left circularly polarized X-rays. In (b) the resultant XMCD and the integrated signal (dashed line) over the spectra. In (c) the sum of both left and right XAS and its respective integrated signal.

not shown). It is, thus, an interesting effect of the interface with Co, since, alone, Gd tends to show a purely ferromagnetic behavior below its Curie temperature.

While the Co spin magnetic moment slightly increases at the Co/Pt interface, it decreases at the interfacial region close to Gd. It is worth noting that the Co atoms are responsible for the IMM in the Pt layers, with a significant induced moment of $\mu_s = 0.22\mu_B$/atom at the Co/Pt interface, while the IMM at the Pt/Gd interface is negligible ($0.05\mu_B$/atom). This can be explained by the fact that the hybridization between Pt and Gd atoms occurs prominently between Pt $5d$ and Gd $5d$, $6p$ and $6s$ valence states, while the Gd $4f$ states, here taken into account by an open-core treatment ($7\mu_B$/atom), are highly localized. Because of this fact, even when the $4f$ states are explicitly taken into account, properly corrected with a Hubbard U approach,[38] the induced Pt spin moment by Gd is still very small (results discussed in the SI). Therefore, based on first-principles calculations, it allows to infer that the IMM in the Pt layers follows the Co magnetic moment, presenting a low influence of the Gd atoms. It is also possible to anticipate that this scenario might not be significantly changed by temperature effects.

With further increasing T, the average theoretical $\bar{\mu}_s^z$ for the Pt, Co and Gd atoms at $T = 300$ K, along with the experimental results obtained from XMCD, are shown in Table 1 and Figure 5(a). The theoretical and experimental results are in excellent agreement, in both magnitude and orientation. At this temperature, the non-zero magnetization observed in the Pt/Co/Gd sample originates mainly in the Co layers, presenting a small IMM in the Pt atoms, and a non-null spin moment in Gd – specially at the interface. Explicitly, the Pt layers follow the Co magnetization with a vanishing IMM of $\sim 0.03\mu_B$/atom and the Gd layers are polarized with a large $\bar{\mu}_s \sim -2.74\mu_B$/atom ferrimagnetic configuration at the Co/Gd interface, where more distant layers present small moments that tend to be antiparallel with the interfacial Gd.

Table 1: Theoretical ($T = 0$ and 300 K) and experimental ($T = 300$ K) average spin ($\bar{\mu}_s$) magnetic moments for Pt, Co and Gd atoms in the Pt/Co/Gd multilayer, in μ_B/atom. Negative/positive signs indicate distinct dynamically averaged moment directions projected in the $\hat{z}$-axis. The minus sign denotes an antiparallel spin orientation.

	Theoretical		**Experimental**
	$T = 0$ K	$T = 300$ K	$T = 300$ K
Pt	0.09	0.03	0.09 ± 0.04
Co	1.85	1.48	1.45 ± 0.02
Gd	-0.18^a	-0.67	-0.54 ± 0.03

a Note that $\bar{\mu}_s \to 0$ due to the almost antiferromagnetic spin configuration throughout the Gd thickness. However, absolute values amount to $\sim 7.6\,\mu_B$/atom (see Figure 5(a)).

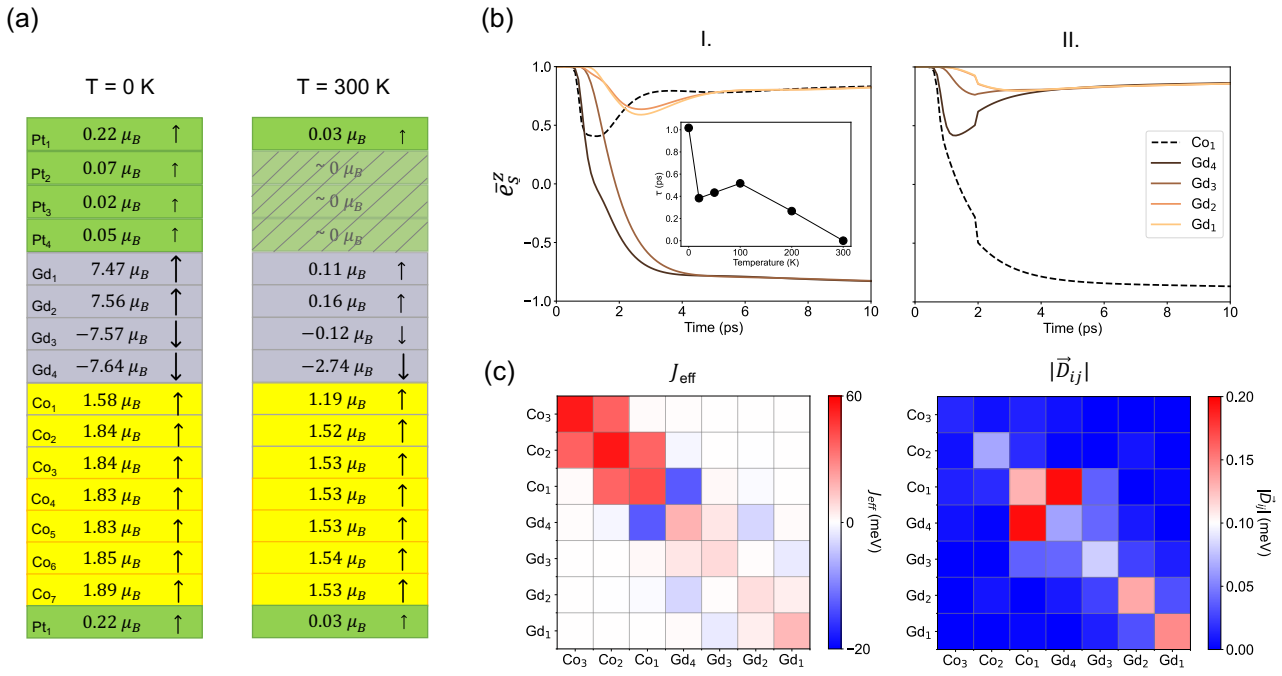

Figure 5: DFT and ASD results for Pt/Co/Gd. In (a), the Pt/Co/Gd stacking is illustrated where the green, gray, and yellow layers represent the Pt, Gd, and Co atoms, respectively. The atomic spin magnetic moments for each layer are indicated along with the direction of polarization (arrow) for 0 K and 300 K. The first Pt layer representation (top) is repeated at the bottom to show the connection with the upcoming Co_7 layer. In (b), the $\hat{z}$-component of the spin moment direction (normalized to a unit vector: $\bar{e}_s^z \in [-1, 1]$) is plotted as a function of time for the Co_1, Gd_4, Gd_3, Gd_2 and Gd_1 layers, considering two different sets of magnetic interactions: complete, depicted in I., and with Gd_4-Gd_1 and Gd_4-Gd_2 interlayer couplings set to zero, depicted in II. In (c), the effective exchange interactions J_{eff} (see main text) and nearest-neighbors $|\vec{D}_{ij}|$ are represented in a color map for different couplings among Gd and the nearest Co layers.

Since experimentally the Pt/Gd multilayer is paramagnetic at this temperature, the Gd moment can be understood in Pt/Co/Gd as being *induced* as well, by proximity with Co. Microscopically, this influence is manifested by an antiferromagnetic exchange coupling between Co and Gd atoms, which quickly vanishes after the nearest-neighboring shell, and is responsible for maintaining a relatively large $\bar{\mu}_s$ at the Gd_4 even at $T = 300$ K; the spin magnetic moment in the other Gd layers rapidly decreases with increasing T (see Figure S12 in SI). Hence, the Co/Gd interface is not only responsible for the antiparallel alignment of Gd w.r.t. Co, but also for the net magnetization in Gd observed at room-temperature. These interfacial effects are instrumental to the existence of a synthetic ferrimagnetic ultrathin region, that may serve as a platform for complex (noncollinear) spin structures and topologically protected states.[39,40]

In addition to the spin moment, another possible point of comparison with the experimental results can be made by considering the orbital magnetic moments, $\bar{\mu}_o$. Although the Gd orbital moment cannot be directly compared with the experimental, because it was quantified for the $4f$ states, while the theoretical treatment for the Gd is acquired in the s, p and d orbitals, the Co orbital magnetic moment is a suitable candidate. Since the orbital magnetic moment of fcc Co does not present a significant variation with temperature,[41] a fair comparison was done between the orbital magnetic moment acquired theoretically as $\sim 0.11\ \mu_B$/atom (at $T = 0$ K), and experimentally as $0.12\ \mu_B$/atom (at $T = 300$ K). Therefore, the theoretical and experimental Co orbital magnetic moments are in excellent agreement.

Up to now, the layer-by-layer *ab-initio* analysis has shown that the magnetization is not homogeneously distributed throughout the thickness of Gd. Although the two closest layers remain in a ferrimagnetic configuration with respect to Co, the other two layers are characterized by an opposite alignment of the magnetization. To demonstrate that dynamically, in Figure 5(b) are presented ASD simulation results where the spin configuration is allowed to relax from the fully saturated state – the equivalent of applying a sufficiently strong external magnetic field, and then suddenly removing it – at very low temperatures ($T = 10^{-3}$ K), and in the overdamped regime ($\alpha = 0.5$). We see that the spin moments Gd_3 and Gd_4 layers quickly proceed to their ferrimagnetic state with respect to Co_1, while, in a later stage, the spin moment $\hat{z}$-component of Gd_2 and Gd_1 reaches a minimum after $\Delta t \sim 3$ ps, gradually converging to a ferromagnetic state with respect to Co_1. Moreover, the simulations show that the transition from the Gd saturated state to the lower-energy configuration in Pt/Co/Gd, for the range of magnetic parameters considered here, occurs dynamically in intervals of ~ 1 ps per layer from $Gd_4 \rightarrow Gd_2/Gd_1$, characterizing an ultrafast process driven by the exchange interactions. A finite temperature analysis on Figure 5(b), *inset*, shows that those intervals decrease with respect to temperature, where the transitions for each Gd layer occur in the same interval of less than 1 ps for $T = 300$ K. In connection to this spin-flip dynamics, we also note that the relevant magnetization switching effect by an external stimuli (e.g., femtosecond laser pulses) was mainly observed in materials involving rare-earth elements.[22,23,26,42]

To closely inspect the microscopic origin of such behavior of Gd, we show in Figure 5(c) the effective exchange among Gd and the nearest Co layers, defined as $J_{\text{eff}} = \sum_{i \neq j} J_{ij}$, which represents the exchange energy term in the spin Hamiltonian for a ferromagnetic (fully saturated) reference state. From this definition, $J_{\text{eff}} > 0$ ($J_{\text{eff}} < 0$) indicates the preference for the parallel (antiparallel) spin alignment. In practice, the intra- and inter-layer exchange interactions were considered up to maximum cutoff radii of ~ 9.6 Å/~ 16 Å, respectively. On one hand, it can be seen in Figure 5(c) that Co influence almost does not exceed the first (adjacent) layer, presenting a strong antiferromagnetic coupling for Co_1-Gd_4. On the other hand, Gd_3-Gd_1 and Gd_4-Gd_2 interlayer J_{eff} parameters are sizable and also negative, with almost the same magnitude of the Gd neighboring layers (with the exception of Gd_3-Gd_2). This particular combination of exchange interactions, favoring longer-range Gd-Gd over

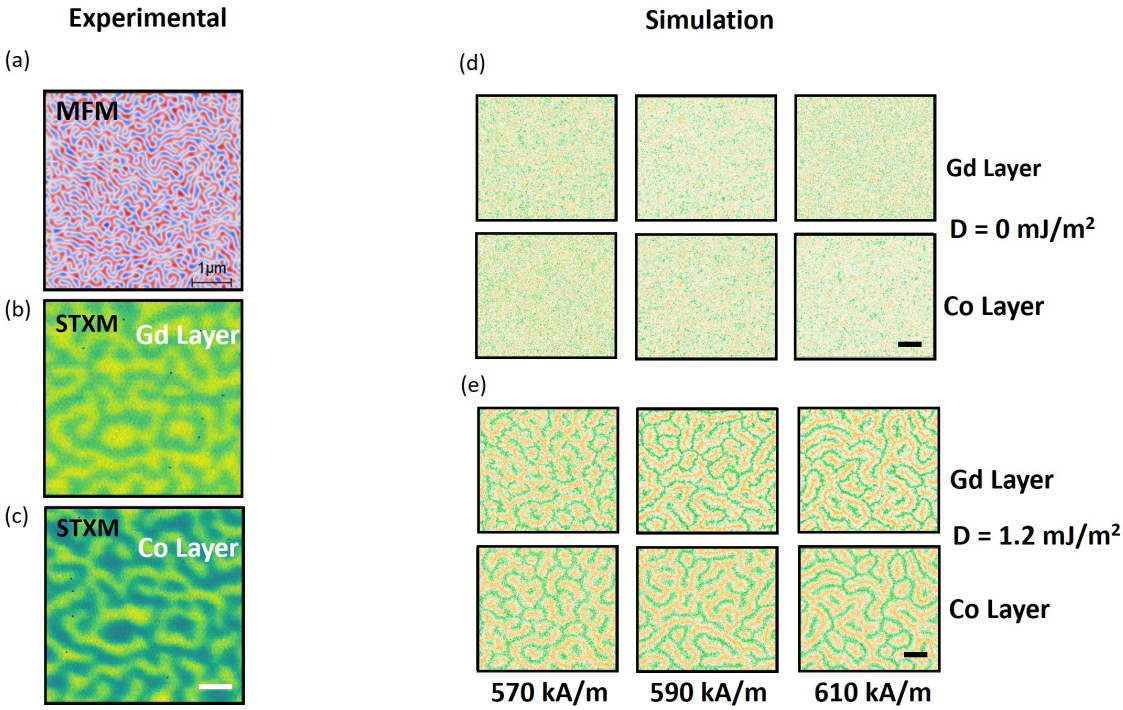

Figure 6: MFM, STXM and micromagnetic simulation images. In (a), the MFM image shows the formation of spin spirals like maze domains. In (b) and (c) STXM images performed at the L_3 Co and M_5 Gd absorption edges show the antiferromagnetic contrast of the two Co and Gd sublattices. The scale bar shown in (c) represents 250 nm. In (d), the micromagnetic simulation was undertaken without DMI, and (e) the spin spirals were reproduced by taking into account DMI in the micromagnetic modeling. The scale bar in (d,e) represents 150 nm.

Gd-Co couplings, is crucial for the preferred FSS derived from the spin Hamiltonian minimization. In this sense, it is worth to recall that in its bulk (hcp) form, Gd exhibits a next-nearest-neighbor antiferromagnetic coupling,[43] being considered as a model example of the indirect Ruderman-Kittel-Kasuya-Yosida (RKKY) interaction;[44] as it is well-known, this type of interactions is mediated by the conduction electrons and presents a long-range nature. On the contrary, fcc Co is an almost strong ferromagnet, for which a less pronouced RKKY character (as well as a faster decaying J_{ij} with the ij-pair distance) is expected.[45]

ASD simulations are performed where the (J_{ij}, $\vec{D}_{ij}$) sets of interactions, namely the Gd_3-Gd_1 and Gd_4-Gd_2 interlayer couplings (antiferromagnetic J_{eff} couplings, represented in blue, in Figure 5(c)), were artificially set to zero. In this case, all Gd layers remained with the same spin alignment. This indicates that there exists a competition between exchange interactions that favors energetically the inhomogeneous magnetization throughout Gd, which is not destroyed by either the influence of thermal fluctuations at $T = 300$ K (see Figure 5(a)), or the weak magnetic anisotropy. More specifically, this behavior can be ascribed to a combination of three connected facts: (*i*) a negligible ferrimagnetic Gd-Co coupling beyond adjacent layers, linked to the (almost) strong ferromagnet character of Co; (*ii*) a small J_{eff} coupling between neighboring Gd_3-Gd_2 layers, which can be easily perturbed by thermal fluctuations; and (*iii*) the presence of long-range, RKKY-type, antiferromagnetic Gd-Gd interlayer interactions.

Finally, it is relevant to note that for the Dzyaloshinskii-Moriya interaction (DMI), exhibited in Figure 5(c), only the Co/Gd interface shows a significant contribution, which is comparable with the intralayer Co_7-Co_7 coupling (see Figure S9 in SI), near the Co/Pt interface. The presence of DMI will be argued to play a central role in the emergence of non-collinear spin structures in the next sections.

Zero-field magnetic textures at room-temperature. Magnetic force microscopy (MFM) images were undertaken at room-temperature and zero magnetic field to observe the formation of magnetic textures in the multilayer. To directly understand the spatial magnetic configuration and correlate with the hysteresis loops, the images were performed with the sample in remnant state after applying a magnetic field of 1 T normal to the sample surface and turning it off. The image shows spin spirals textures in the format of maze-like domains, depicted in Figure 6(a). Recalling the hysteresis loops presented in Figure 2(b), the almost zero remnant magnetization agrees with the observed images, where the sample magnetization breaks into narrow domains with up and down orientation, reducing the average magnetization of the multilayer in the absence of magnetic field.

The MFM images confirm the magnetic textures formation in the multilayer. However, the MFM cannot itself directly answer if the magnetic textures are formed in both Co and Gd layers. To obtain the domains formation in each Co and Gd layer, Scanning transmission X-ray microscopy (STXM) measurements were performed at the 7.0.1.2 (COSMIC) beamline of the Advanced Light Source (ALS) synchrotron. To transmit the X-ray through the sample, the same Pt(1nm)/Co(1.5nm) multilayer was grown onto transparent silicon nitride Si_3N_4 membranes. Right and left circularly polarized X-rays were used with the incoming energy fixed at the maximum of both Co L_3 and Gd M_5 absorption edge. The magnetic contrast was obtained based on XMCD, through the difference between images performed with right and left circularly polarization at room-temperature and zero-magnetic field. Figure 6(b-c) shows the formation of spin spirals in each Gd and Co thicknesses with a very similar pattern obtained by MFM. Moreover, the contrast is opposite for each Co and Gd XMCD images, which confirms that the spin spirals texture at zero-field are coupled ferrimagnetically. These domains may be transformed in ferrimagnetic skyrmions in Pt/Co/Gd multilayer at zero-field and room temperature, by tailoring circular shaped disks with different diameters,[46] or by tuning perpendicular magnetic

anisotropy and remnant magnetization varying the Co thickness.[47]

Theoretical analysis: Micromagnetic simulations. The observation of ferrimagnetically coupled spin spirals by both MFM and STXM in our Pt/Co/Gd multilayer, with wavelengths of, roughly, 100 nm order of magnitude (see Fig. 6) makes the fully atomistic treatment unpractical. Therefore, following the philosophy of a multiscale approach,[48] the formation of those spin spirals was deeply investigated by, instead, performing micromagnetic simulations[1] using Mumax^3 code[49] (for details see Methods section).

Figure 6(d-e) summarizes the main micromagnetic results. In the bottom of Figure 6(e) is labeled different values of saturation magnetization M_s to verify how the domain structures evolve as a function of this parameter. The spin textures were stabilized in both micromagnetic Co and Gd layers. When the DMI is absent in the micromagnetic modeling ($D = 0$), no domain textures were stabilized, while for $D = 1.2 \times 10^{-3}$ J/m^2 spin spirals like maze-domains are obtained, as observed experimentally. By modifying the values of DMI, the micromagnetic simulations allowed to qualitatively estimate this substantial interaction where the images match with the experimental findings. The range of DMI from $1.1 - 1.4 \times 10^{-3}$ J/m^2 reproduces very well the experimental observations. Furthermore, no significant difference in the micromagnetic images was observed within the M_s interval of 570 to 610 kA/m, as well as the $J_{\text{Co-Gd}}$ interaction from -0.1 to 0.7×10^{-3} J/m^2.

Conclusions

In conclusion, various interfacial phenomena such as induced magnetic moments, exchange coupling, and spin textures were comprehensively explored in Pt/Co/Gd multilayers at both zero and room-temperatures by employing a multiscale approach. Our combined experimental and theoretical analysis, supported by XMCD, DFT, and ASD simulations, reveals that the Gd in proximity with Co leads to essentially two local effects: (i) the presence of a sizable, induced magnetic moment transferred from Co to Gd, which is ferrimagnetic with respect to Co at the Gd/Co interface, and still survives at $T = 300$ K; and (ii) the emergence of a flipped spin state (FSS) throughout the Gd layers when the ideal fcc structure with Pt lattice parameter is considered. The FSS, characterized by a distinct alignment of Gd magnetic moments (antiparallel to Co near the interface and parallel far from it), is mainly driven by the long-range (RKKY-type) Gd-Gd exchange interactions and the shorter-range influence of Co, in an environment of weak uniaxial anisotropy. The FSS across the Gd layer reduces its thickness normalized magnetic moment sustained by both experimental and theoretical results. Moreover, the Pt layers are found to predominantly follow the magnetic moment direction of Co near the Co/Pt interface, with minimal induced moments in proximity to Gd atoms.

On a larger scale, the presence of the Co layers breaks the system's inversion symmetry, leading to the appearance of DMI specially at the Co/Pt and Co/Gd interfaces, via Co-Co and Co-Gd interactions, respectively. The DMI is demonstrated, via micromagnetic simulations, to play a crucial role on the formation of ferrimagnetically coupled spin spirals, observed by MFM and STXM techniques at room-temperature. This observation further underscores the complexity and richness of the magnetic configurations in this system. These conclusions enhance our understanding of interfacial magnetic properties in such heterostructures, and offer deeper insights toward the manipulation and control of antiferromagnetic coupled magnetic states, which are critical for advancements in ultra-low power data storage, photonics, and spintronic applications.

Methods

Sample fabrication

Magnetic multilayers were fabricated by mag-

[1] Note here we differentiate the atomistic parameters J_{ij} and $\vec{D}_{ij}$ used in the ASD simulations, from the effective parameters J and D used in the micromagnetic simulations.

netron sputtering at room-temperature with a base pressure of 8×10^{-8} Torr. All targets were deposited onto Si/SiO_2 substrates under Argon atmosphere pressure of 3×10^{-3} Torr. First, two reference Pt(1nm)/Gd(1nm) and Pt(1nm)/Co(1.5nm) multilayers were grown. The bi-layers were grown with 10 repetitions over 2 nm Pt buffer layer, and to prevent oxidation 2 nm Pt thickness was added upon the last repetition of the bi-layers. Thus, the Co and Gd thicknesses were sandwiched at both sides by the Pt forming a symmetric Pt/Co/Pt and Pt/Gd/Pt heterostructure. Thus, a multilayer based on Pt(1nm)/Co(1.5nm)/Gd(1nm) with ten repetions was fabricated to study the magnetic-coupling between adjacentes Co and Gd atoms, as well as the formation of spin textures in both magnetic layers.

Theoretical multiscale approach:

1: Atomistic spin dynamics

To perform first-principles calculations the the real-space linear-muffin-tin-orbital within the atomic sphere approximation (RS-LMTO-ASA) method,[50] based on the Density Functional Theory (DFT)[51] was used. The ground state electronic density was obtained by using the Haydock recursion,[52] with the recursion cut-off of $LL = 22$, in addition to the Beer-Perttifor terminator[53] and the local spin density approximation (LSDA)[54] as the exchange-correlation functional. The atomistic spin simulations were done using the Uppsala Atomistic Spin Dynamics (UppASD)[55] code, where the Landau-Lifshitz-Gilbert (LLG) equation[56] is solved to obtain the magnetic configuration with minimum energy.

An infinite geometry with perfect *fcc* stacking in the [111] direction, composed by 4 layers of Pt, 4 layers of Gd, and 7 layers of Co (see Figure 5(a)) was considered. The DFT calculations were performed using the Real Space Linear Muffin-Tin Orbital Atomic Sphere Approximation (RS-LMTO-ASA) method[50,57–67] to obtain the magnetic parameters, including magnetic moments and exchange constants, namely the isotropic exchange coupling (J_{ij}) and the Dzyaloshinskii-Moriya vectors ($\vec{D}_{ij}$). A deeper analysis on the structure and the ground-state search using different DFT methods can be found in the SI. Subsequently, the obtained *ab-initio* values were used to parametrize the spin Hamiltonian and solve the phenomenological Landau-Lifshitz-Gilbert (LLG) equation of motion, with temperature variations from ~ 0 to 300 K, via the Uppsala Atomistic Spin Dynamics (UppASD) code.[55,68,69]

Concerning the ASD simulations, the inclusion of induced magnetic moments can be crucial for the determination of T_C and the magnetic properties at finite temperatures of FM/heavy-metal systems.[70] However, since the IMM for Pt layers is only sizable at the interface Pt/Co (as discussed below, see Figure 5(a)), including further Pt atoms with vanishing small magnetic moments in the classical ASD approach is not appropriate.[71] Then, here, we considered a hexagonal lattice of $200 \times 200 \times n$ spins, where n is the number of layers, considering one Pt monolayer at the interface Pt/Co followed by all the Co and Gd layers, resulting in $n = 12$ (see SI for information regarding the range of interactions considered). The temperature is increased continuously from 0 K to 300 K, where the atomic moments present a deviation of the $\hat{z}$-axis due to thermal fluctuations. As the XMCD results consider contributions from all the layers of a given chemical species (for Co and Gd, only the repetitions closest to the sample surface due the TEY mode detection, see Figure 2(a)),[72] a fair comparison to the theoretical values can be given by the *average projection* of the atomic spins to the spin quantization axis ($\hat{z}$-axis), $\bar{\mu}_s^z$. For the cases in which a finite temperature ($T > 0$) is involved, these values are obtained by considering the dynamical average $\hat{z}$-component of $\vec{\mu}_{s_i}$ for all sites i in a given layer, for a sufficient ASD simulation time of $t = 10$ ps.

2: Micromagnetic simulations

Within the micromagnetic approach, to model our system, using Mumax^3 code,[49] two layers representing Co and Gd were geometrically divided into cell sizes of 0.3 nm along the $\hat{x} - \hat{y}$ plane, and 0.5 nm out-of-plane ($\hat{z}$). The total area along $\hat{x} - \hat{y}$ is 750×750 nm^2, and Co and Gd thicknesses 1.5 and 1 nm along the $\hat{z}$ direction, respectively. The simulations were carried out at $T = 300$ K, zero field and during $t = 10$ ns.

The exchange stiffness constant was fixed to $J_{\text{Co-Co}} = 1.5 \times 10^{-12}$ J/m^3 and $J_{\text{Gd-Gd}} = 0.5 \times 10^{-12}$ J/m^3.[18] The antiparallel alignment between the Co and Gd layers in the interface was ensured by using interlayer exchange coupling (IEC), mimicking an interfacial exchange $J_{\text{Co-Gd}}$ interaction for the nearest Co and Gd atoms. The $J_{\text{Co-Gd}}$ was initially fixed in -0.5×10^{-3} J/m^2. The PMA obtained experimentally was fixed in 0.12 MJ/m^3 and saturation magnetization modified from 570 to 610 kA/m to account for any variation of this parameter in for-

mation of the magnetic texture. As the atomistic results previously discussed suggest, a sizable DMI is also present due to the broken inversion symmetry structure. Thus, a DMI constant D was also considered in the simulations and varied together with the interfacial exchange $J_{Co\text{-}Gd}$ to explore their impact on the spin textures emergence. Additional results of micromagnetic simulations are described in the SI.

Acknowledgement J.B, J.C.C, F.B, T.J.A.M, H.M.P, A.B.K, and P.C.C. acknowledge financial support from Brazilian agencies CAPES, CNPq, FAPESP and FAPESPA. In particular, São Paulo Research Foundation (FAPESP) is acknowledged by financial support through the processes: #2020/05609-7 and #2022/10095-8 (P.C.C., A.B.K. and H.M.P), #2012/51198-2 (J.C.C). A.B.K. acknowledges support from the INCT of Materials Informatics, and A.B.K., J.B., T.J.A.M., F.B. and J.C.C. acknowledge the INCT of Spintronics and Advanced Magnetic Nanostructures (INCT-SpinNanoMag). A.B. acknowledges eSSENCE. A.B. and I.P.M. acknowledge support from the Knut and Alice Wallenberg Foundation. F.B acknowledges support from CNPq project with process number #421070/2023-4. XAS and XMCD measurements were carried out thanks to the beamtime in the U11-PGM beamline of the Brazilian Synchrotron Light Laboratory (LNLS/CNPEM), as well as the Extreme Condition Analyses (EMA) beamline. The calculations were performed at the computational facilities of the National Laboratory for Scientific Computing (LNCC/MCTI, Brazil), CCAD-UFPA (Brazil), and at the National Academic Infrastructure for Supercomputing in Sweden (NAISS, projects 2023/1-44, 2023/1-10, 2023/5-454, and 2023/22-1107) at both the National Supercomputing Centre (NSC, Tetralith) and the PDC Centre for High Performance Computing (PDC-KTH, Dardel).

Supporting information

Additional description of the experimental and theoretical details, including: (*i*) X-ray diffraction to identify the growth direction of the thin films, X-ray absorption and the sum rules used to obtain the orbital and spin magnetic moments, and (*ii*) the computational procedure to perform first principles calculations based on density functional theory (DFT), and atomistic spin dynamics. Besides, further information on the micromagnetic simulations are presented.

Competing interests

All the authors declare no competing interests.

Author contributions

J.B. conceived the experimental idea of the projetc. I.P.M., A.B.K., and H.M.P. designed the theoretical project. P.C.C, I.P.M., J.B., and A.B.K. carried out the simulations and calculations. I.P.M. and A.B. developed new implementations on RS-LMTO-ASA code necessary to develop this project. J.B., T.J.A.M., and J.C.C. performed the XAS and XMCD experiments. T.J.A.M. undertook STXM images. F.B. and J.B measured hysteresis loops. The initial version of the manuscript was written by J.B., P.C.C., I.P.M., and A.B.K. A.B., H.M.P., and J.C.C. discussed the results and commented on the manuscript. All authors contributed to discussions, writing, and revision of the manuscript to its final version.

Data availability

Most data needed to reproduce the results are available in the SI. Additional details supporting the findings of this study can be provided upon reasonable request from the corresponding authors (J.B. and I.P.M.).

Code availability

The codes used in the theoretical part (RS-LMTO-ASA, UppASD, and Mumax[3]) are described and referenced in the Methods section and are available free-of-charge.

References

(1) Huang, S. Y.; Fan, X.; Qu, D.; Chen, Y. P.; Wang, W. G.; Wu, J.; Chen, T. Y.; Xiao, J. Q.; Chien, C. L. Transport Magnetic Proximity Effects in Platinum. *Phys. Rev. Lett.* **2012**, *109*, 107204.

(2) Hellman, F. et al. Interface-induced phenomena in magnetism. *Rev. Mod. Phys.* **2017**, *89*, 025006.

(3) Nguyen, M.-H.; Pai, C.-F.; Nguyen, K. X.; Muller, D. A.; Ralph, D. C.; Buhrman, R. A. Enhancement of the anti-damping spin torque efficacy of platinum by interface modification. *Appl. Phys. Lett.* **2015**, *106*, 222402.

(4) Zhang, W.; Han, W.; Jiang, X.; Yang, S.-H.; S. P. Parkin, S. Role of transparency of platinum–ferromagnet interfaces in determining the intrinsic magnitude of the spin Hall effect. *Nat. Phys.* **2015**, *11*, 496.

(5) Buzdin, A. I. Proximity effects in superconductor-ferromagnet heterostructures. *Rev. Mod. Phys.* **2005**, *77*, 935.

(6) Lutchyn, R. M.; Sau, J. D.; Das Sarma, S. Majorana Fermions and a Topological Phase Transition in Semiconductor-Superconductor Heterostructures. *Phys. Rev. Lett.* **2010**, *105*, 077001.

(7) Shabani, J.; Kjaergaard, M.; Suominen, H. J.; Kim, Y.; Nichele, F.; Pakrouski, K.; Stankevic, T.; Lutchyn, R. M.; Krogstrup, P.; Feidenhans'l, R.; Kraemer, S.; Nayak, C.; Troyer, M.; Marcus, C. M.; Palmstrøm, C. J. Two-dimensional epitaxial superconductor-semiconductor heterostructures: A platform for topological superconducting networks. *Phys. Rev. B* **2016**, *93*, 155402.

(8) Vogel, J.; Fontaine, A.; Cros, V.; Petroff, F.; Kappler, J.-P.; Krill, G.; Rogalev, A.; Goulon, J. Structure and magnetism of Pd in Pd/Fe multilayers studied by x-ray magnetic circular dichroism at the Pd $L_{2,3}$sedges. *Phys. Rev. B* **1997**, *55*, 3663.

(9) Wilhelm, F.; Poulopoulos, P.; Ceballos, G.; Wende, H.; Baberschke, K.; Srivastava, P.; Benea, D.; Ebert, H.; Angelakeris, M.; Flevaris, N. K.; Niarchos, D.; Rogalev, A.; Brookes, N. B. Layer-Resolved Magnetic Moments in Ni/Pt Multilayers. *Phys. Rev. Lett.* **2000**, *85*, 413.

(10) Wilhelm, F.; Poulopoulos, P.; Wende, H.; Scherz, A.; Baberschke, K.; Angelakeris, M.; Flevaris, N. K.; Rogalev, A. Systematics of the Induced Magnetic Moments in 5*d* Layers and the Violation of the Third Hund's Rule. *Phys. Rev. Lett.* **2001**, *87*, 207202.

(11) Hase, T. P. A.; Brewer, M. S.; Arnalds, U. B.; Ahlberg, M.; Kapaklis, V.; Björck, M.; Bouchenoire, L.; Thompson, P.; Haskel, D.; Choi, Y.; Lang, J.; Sánchez-Hanke, C.; Hjörvarsson, B. Proximity effects on dimensionality and magnetic ordering in Pd/Fe/Pd trialyers. *Phys. Rev. B* **2014**, *90*, 104403.

(12) Lu, Y. M.; Choi, Y.; Ortega, C. M.; Cheng, X. M.; Cai, J. W.; Huang, S. Y.; Sun, L.; Chien, C. L. Pt Magnetic Polarization on $\mathbf{Y}_3\mathrm{Fe}_5\mathbf{O}_{12}$ and Magnetotransport Characteristics. *Phys. Rev. Lett.* **2013**, *110*, 147207.

(13) Collet, M.; Mattana, R.; Moussy, J.-B.; Ollefs, K.; Collin, S.; Deranlot, C.; Anane, A.; Cros, V.; Petroff, F.; Wilhelm, F.; Rogalev, A. Investigating magnetic proximity effects at ferrite/Pt interfaces. *Appl. Phys. Lett.* **2017**, *111*, 202401.

(14) Swindells, C.; Nicholson, B.; Inyang, O.; Choi, Y.; Hase, T.; Atkinson, D. Proximity-induced magnetism in Pt layered with rare-earth–transition-metal ferrimagnetic alloys. *Phys. Rev. Res.* **2020**, *2*, 033280.

(15) Stanciu, C. D.; Hansteen, F.; Kimel, A. V.; Kirilyuk, A.; Tsukamoto, A.; Itoh, A.; Rasing, T. All-Optical Magnetic Recording with Circularly Polarized Light. *Phys. Rev. Lett.* **2007**, *99*, 047601.

(16) Lalieu, M. L. M.; Peeters, M. J. G.; Haenen, S. R. R.; Lavrijsen, R.; Koopmans, B. Deterministic all-optical switching of synthetic ferrimagnets using single femtosecond laser pulses. *Phys. Rev. B* **2017**, *96*, 220411.

(17) Hirata, Y.; Kim, D.; Kim, S. Vanishing skyrmion Hall effect at the angular momentum compensation temperature of a ferrimagnet. *Nat. Nanotechnol.* **2019**, *14*, 232.

(18) Woo, S. et al. Current-driven dynamics and inhibition of the skyrmion Hall effect of ferrimagnetic skyrmions in GdFeCo films. *Nat. Commun.* **2018**, *9*, 959.

(19) Siddiqui, S. A.; Han, J.; Finley, J. T.; Ross, C. A.; Liu, L. Current-Induced Domain Wall Motion in a Compensated Ferrimagnet. *Phys. Rev. Lett.* **2018**, *121*, 057701.

(20) Wienholdt, S.; Hinzke, D.; Nowak, U. THz Switching of Antiferromagnets and Ferrimagnets. *Phys. Rev. Lett.* **2012**, *108*, 247207.

(21) Blank, T. G. H.; Grishunin, K. A.; Mashkovich, E. A.; Logunov, M. V.; Zvezdin, A. K.; Kimel, A. V. THz-Scale Field-Induced Spin Dynamics in Ferrimagnetic Iron Garnets. *Phys. Rev. Lett.* **2021**, *127*, 037203.

(22) Radu, I.; Vahaplar, C., K. Stamm; Kachel, T.; Pontius, H. A., N. Dürr; Ostler, T. A.; Barker, J.; Evans, R. F. L.; Chantrell, R. W.; Tsukamoto, A.; Itoh, A.; Kirilyuk, A.; Rasing, T.; Kimel, A. V. Transient ferromagnetic-like state mediating ultrafast reversal of antiferromagnetically coupled spins. *Nat.* **2011**, *472*, 205.

(23) Ostler, T. et al. Ultrafast heating as a sufficient stimulus for magnetization reversal in a ferrimagnet. *Nat. Commun.* **2012**, *3*, 666.

(24) Zhang, W.; Huang, T. X.; Hehn, M.; Malinowski, G.; Verges, M.; Hohlfeld, J.; Remy, Q.; Lacour, D.; Wang, X. R.; Zhao, G. P.; Vallobra, P.; Xu, Y.; Mangin, S.; Zhao, W. S. Optical Creation of Skyrmions by Spin Reorientation Transition in Ferrimagnetic CoHo Alloys. *ACS Appl. Mater. Interfaces* **2023**, *15*, 5608.

(25) Zhu, K.; Bi, L.; Zhang, Y.; Zheng, D.; Yang, D.; Li, J.; Tian, H.; Cai, J.; Yang, H.; Zhang, Y.; Li, J. Ultrafast switching to zero field topological spin textures in ferrimagnetic TbFeCo films. *Nanoscale* **2024**, *16*, 3133.

(26) Gweha Nyoma, D. P.; Hehn, M.; Malinowski, G.; Ghanbaja, J.; Hohlfeld, J.; Gorchon, J.; Mangin, S.; Montaigne, F. Gd Doping at the Co/Pt Interfaces to Induce Ultrafast All-Optical Switching. *ACS Appl. Electron. Mater.* **2024**, *6*, 1122.

(27) Smejkal, L.; Mokrousov, Y.; Yan, B.; MacDonald, A. H. Topological antiferromagnetic spintronics. *Nat. Phys.* **2018**, *14*, 242–251.

(28) Baltz, V.; Manchon, A.; Tsoi, M.; Moriyama, T.; Ono, T.; Tserkovnyak, Y. Antiferromagnetic spintronics. *Rev. Mod. Phys.* **2018**, *90*, 015005.

(29) Gomonay, O.; Baltz, V.; Brataas, A.; Tserkovnyak, Y. Antiferromagnetic spin textures and dynamics. *Nat. Phys.* **2018**, *14*, 213.

(30) Binder, M.; Weber, A.; Mosendz, O.; Woltersdorf, G.; Izquierdo, M.; Neudecker, I.; Dahn, J. R.; Hatchard, T. D.; Thiele, J.-U.; Back, C. H.; Scheinfein, M. R. Magnetization dynamics of the ferrimagnet CoGd near the compensation of magnetization and angular momentum. *Phys. Rev. B* **2006**, *74*, 134404.

(31) Kim, J.; Lee, D.; Lee, K.-J.; Ju, B.-K.; Koo, H. C.; Min, B.-C.; Lee, O. Spin-orbit torques associated with ferrimagnetic order in Pt/GdFeCo/MgO layers. *Sci. Rep.* **2018**, *8*, 6017.

(32) Coey, J. M. D. *Magnetism and Magnetic Materials*; Cambridge University Press, 2010.

(33) Strigl, F.; Espy, C.; Bückle, M.; Scheer, E.; Pietsch, T. Emerging magnetic order in platinum atomic contacts and chains. *Phys. Rev. B* **2015**, *6*, 6172.

(34) Verna, A.; Alippi, P.; Offi, F.; Barucca, G.; Varvaro, G.; Agostinelli, E.; Albrecht, M.; Rutkowski, B.; Ruocco, A.; Paoloni, D.; Valvidares, M.; Laureti, S. Disclosing the Nature of Asymmetric Interface Magnetism in Co/Pt Multilayers. *ACS Appl. Mater. Interfaces* **2022**, *14*, 12766.

(35) Mukhopadhyay, A.; Koyiloth Vayalil, S.; Graulich, D.; Ahamed, I.; Francoual, S.; Kashyap, A.; Kuschel, T.; Anil Kumar, P. S. Asymmetric modification of the magnetic proximity effect in Pt/Co/Pt trilayers by the insertion of a Ta buffer layer. *Phys. Rev. B* **2020**, *102*, 144435.

(36) Bartelt, A. F.; Comin, A.; Feng, J.; Nasiatka, J. R.; Eimüller, T.; Ludescher, B.; Schütz, G.; Padmore, H. A.; Young, A. T.; Scholl, A. Element-specific spin and orbital momentum dynamics of Fe/Gd multilayers. *App. Phys. Lett.* **2007**, *90*, 162503.

(37) Jensen, J.; Mackintosh, A. R. *Rare Earth Magnetism*; Clarence Press, 1991.

(38) Dudarev, S. L.; Botton, G. A.; Savrasov, S. Y.; Humphreys, C. J.; Sutton, A. P. Electron-energy-loss spectra and

the structural stability of nickel oxide: An LSDA+U study. *Phys. Rev. B* **1998**, *57*, 1505.

(39) Šmejkal, L.; Mokrousov, Y.; Yan, B.; MacDonald, A. H. Topological antiferromagnetic spintronics. *Nat. Phys.* **2018**, *14*, 242.

(40) Aldarawsheh, A.; Fernandes, I. L.; Brinker, S.; Sallermann, M.; Abusaa, M.; Blügel, S.; Lounis, S. Emergence of zero-field non-synthetic single and interchained antiferromagnetic skyrmions in thin films. *Nat. Commun.* **2022**, *13*, 7369.

(41) Menzinger, F.; Paoletti, A. Temperature dependence of magnetic-moment distribution in f.c.c. CO0.91FE0.09 alloy. *Il Nuovo Cimento B* **1972**, *10*, 565.

(42) Hintermayr, J.; Li, P.; Rosenkamp, R.; van Hees, Y. L. W.; Igarashi, J.; Mangin, S.; Lavrijsen, R.; Malinowski, G.; Koopmans, B. Ultrafast single-pulse all-optical switching in synthetic ferrimagnetic Tb/Co/Gd multilayers. *Appl. Phys. Lett.* **2023**, *123*, 072406.

(43) Locht, I. L. M.; Kvashnin, Y. O.; Rodrigues, D. C. M.; Pereiro, M.; Bergman, A.; Bergqvist, L.; Lichtenstein, A. I.; Katsnelson, M. I.; Delin, A.; Klautau, A. B.; Johansson, B.; Di Marco, I.; Eriksson, O. Standard model of the rare earths analyzed from the Hubbard I approximation. *Phys. Rev. B* **2016**, *94*, 085137.

(44) Scheie, A.; Laurell, P.; McClarty, P. A.; Granroth, G. E.; Stone, M. B.; Moessner, R.; Nagler, S. E. Spin-exchange Hamiltonian and topological degeneracies in elemental gadolinium. *Phys. Rev. B* **2022**, *105*, 104402.

(45) Pajda, M.; Kudrnovský, J.; Turek, I.; Drchal, V.; Bruno, P. Ab initio calculations of exchange interactions, spin-wave stiffness constants, and Curie temperatures of Fe, Co, and Ni. *Phys. Rev. B* **2001**, *64*, 174402.

(46) Brandão, J.; Dugato, D. A.; Puydinger dos Santos, M. V.; Cezar, J. C. Evolution of Zero-Field Ferrimagnetic Domains and Skyrmions in Exchange-Coupled Pt/CoGd/Pt Confined Nanostructures: Implications for Antiferromagnetic Devices. *ACS Appl. Nano Mater.* **2019**, *2*, 7532.

(47) Brandão, J.; Dugato, D.; Puydinger dos Santos, M.; Béron, F.; Cezar, J. Tuning isolated zero-field skyrmions and spin spirals at room-temperature in synthetic ferrimagnetic multilayers. *Appl. Surf. Sci.* **2022**, *585*, 152598.

(48) Borisov, V.; Salehi, N.; Pereiro, M.; Delin, A.; Eriksson, O. Dzyaloshinskii-Moriya interactions, Néel skyrmions and V_4 magnetic clusters in multiferroic lacunar spinel GaV_4S_8. *Npj Comput. Mater.* **2024**, *10*, 53.

(49) Vansteenkiste, A.; Van de Wiele, B. MuMax: A new high-performance micromagnetic simulation tool. *J. Magn. Magn. Mater.* **2011**, *323*, 2585.

(50) Frota-Pessôa, S. First-principles real-space linear-muffin-tin-orbital calculations of 3d impurities in Cu. *Phys. Rev. B* **1992**, *46*, 14570.

(51) Hohenberg, P.; Kohn, W. Inhomogeneous Electron Gas. *Phys. Rev.* **1964**, *136*, B864.

(52) Haydock, R. The recursive solution of the Schrödinger equation. *Comput. Phys. Commun.* **1980**, *20*, 11 – 16.

(53) Beer, N.; Pettifor, D. G. *The Electronic Structure of Complex Systems*; Springer US, 1984.

(54) von Barth, U.; Hedin, L. A Local Exchange-Correlation Potential for the Spin Polarized Case: I. *J. Phys. C Solid State Phys.* **1972**, *5*, 1629.

(55) Eriksson, O.; Bergman, A.; Bergqvist, L.; Hellsvik, J. *Atomistic Spin Dynamics: Foundations and Applications*; Oxford University Press: Oxford, 2017; p 272.

(56) Gilbert, T. A phenomenological theory of damping in ferromagnetic materials. *IEEE Transactions on Magnetics* **2004**, *40*, 3443.

(57) Peduto, P. R.; Frota-Pessôa, S.; Methfessel, M. S. First-principles linear muffin-tin orbital atomic-sphere approximation calculations in real space. *Phys. Rev. B* **1991**, *44*, 13283.

(58) Klautau, A. B.; Legoas, S. B.; Muniz, R. B.; Frota-Pessôa, S. Magnetic behavior of thin Cr layers sandwiched by Fe. *Phys. Rev. B* **1999**, *60*, 3421.

(59) Rodrigues, D. C. M.; Szilva, A.; Klautau, A. B.; Bergman, A.; Eriksson, O.; Etz, C. Finite-temperature interatomic exchange and magnon softening in Fe overlayers on Ir(001). *Phys. Rev. B* **2016**, *94*, 014413.

(60) Bezerra-Neto, M. M.; Ribeiro, M. S.; Sanyal, B.; Bergman, A.; Muniz, R. B.; Eriksson, O.; Klautau, A. B. Complex magnetic structure of clusters and chains of Ni and Fe on Pt(111). *Sci. Rep.* **2013**, *3*, 3054.

(61) Cardias, R.; Bezerra-Neto, M. M.; Ribeiro, M. S.; Bergman, A.; Szilva, A.; Eriksson, O.; Klautau, A. B. Magnetic and electronic structure of Mn nanostructures on Ag(111) and Au(111). *Phys. Rev. B* **2016**, *93*, 014438.

(62) Kvashnin, Y. O.; Cardias, R.; Szilva, A.; Di Marco, I.; Katsnelson, M. I.; Lichtenstein, A. I.; Nordström, L.; Klautau, A. B.; Eriksson, O. Microscopic Origin of Heisenberg and Non-Heisenberg Exchange Interactions in Ferromagnetic bcc Fe. *Phys. Rev. Lett.* **2016**, *116*, 217202.

(63) Cardias, R.; Bergman, A.; Szilva, A.; Kvashnin, Y. O.; Fransson, J.; Klautau, A. B.; Eriksson, O.; Nordström, L. First-principles Dzyaloshinskii–Moriya interaction in a non-collinear framework. *Sci. Rep.* **2020**, *10*, 20339.

(64) Klautau, A. B.; Frota-Pessôa, S. Magnetic properties of Co nanowires on Cu(001) surfaces. *Phys. Rev. B* **2004**, *70*, 193407.

(65) Klautau, A.; Frota-Pessôa, S. Orbital moments of 3d adatoms and Co nanostructures on Cu(001) surfaces. *Surf. Sci.* **2005**, *579*, 27.

(66) Frota-Pessôa, S.; Klautau, A. B.; Legoas, S. B. Influence of interface mixing on the magnetic properties of Ni/Pt multilayers. *Phys. Rev. B* **2002**, *66*, 132416.

(67) Klautau, A.; Frota-Pessôa, S. Magnetism of Co clusters embedded in Cu(001) surfaces: an ab initio study. *Surf. Sci.* **2002**, *497*, 385.

(68) Antropov, V. P.; Katsnelson, M. I.; Harmon, B. N.; van Schilfgaarde, M.; Kusnezov, D. Spin dynamics in magnets: Equation of motion and finite temperature effects. *Phys. Rev. B* **1996**, *54*, 1019.

(69) Skubic, B.; Hellsvik, J.; Nordström, L.; Eriksson, O. A method for atomistic spin dynamics simulations: implementation and examples. *J. Condens. Matter Phys.* **2008**, *20*, 315203.

(70) Polesya, S.; Mankovsky, S.; Sipr, O.; Meindl, W.; Strunk, C.; Ebert, H. Finite-temperature magnetism of Fe_xPd_{1-x} and Co_xPt_{1-x} alloys. *Phys. Rev. B* **2010**, *82*, 214409.

(71) Millard, K.; Leff, H. S. Infinite-Spin Limit of the Quantum Heisenberg Model. *J. Math. Phys.* **1971**, *12*, 1000.

(72) Stöhr, J. X-ray magnetic circular dichroism spectroscopy of transition metal thin films. *J. Electron Spectros. Relat. Phenomena* **1995**, *75*, 253.